π-Flux Dirac Bosons and Topological Edge Excitations in a Bosonic Chiral p-Wave Superfluid

Zhi-Fang Xu, Li You, Andreas Hemmerich, and W. Vincent Liu

Phys. Rev. Lett. **117**, 085301 — Published 15 August 2016

DOI: 10.1103/PhysRevLett.117.085301

π-flux Dirac bosons and topological edge excitations in a bosonic chiral p-wave superfluid

Zhi-Fang Xu,[1,*] Li You,[2,3] Andreas Hemmerich,[4,5] and W. Vincent Liu[6,5,7,†]

[1] *MOE Key Laboratory of Fundamental Physical Quantities Measurements, School of Physics, Huazhong University of Science and Technology, Wuhan 430074, China*
[2] *State Key Laboratory of Low Dimensional Quantum Physics, Department of Physics, Tsinghua University, Beijing 100084, China*
[3] *Collaborative Innovation Center of Quantum Matter, Beijing 100084, China*
[4] *Institut für Laser-Physik, Universität Hamburg, Luruper Chaussee 149, 22761 Hamburg, Germany*
[5] *Wilczek Quantum Center, Zhejiang University of Technology, Hangzhou 310023, China*
[6] *Department of Physics and Astronomy, University of Pittsburgh, Pittsburgh, Pennsylvania 15260, USA*
[7] *Center for Cold Atom Physics, Chinese Academy of Sciences, Wuhan 430071, China*

We study the topological properties of elementary excitations in a staggered $p_x \pm ip_y$ Bose-Einstein condensate realized in recent orbital optical lattice experiments. The condensate wave function may be viewed as a configuration space variant of the famous p_x+ip_y momentum space order parameter of strontium ruthenate superconductors. We show that its elementary excitation spectrum possesses Dirac bosons with π Berry flux. Remarkably, if we induce a population imbalance between the $p_x + ip_y$ and $p_x - ip_y$ condensate components, a gap opens up in the excitation spectrum resulting in a nonzero Chern invariant and topologically protected edge excitation modes. We give a detailed description on how our proposal can be implemented with standard experimental technology.

Introduction. In quantum gases, the current focus on topological features so far has been directed towards fermionic atoms, whose phase diagrams often are easily obtained, thanks to extensive knowledge derived from analogous electron models [1, 2]. Consorted efforts in cold atom physics aim at simulating famous electronic topological models that are non-interacting but possess geometric phases [3–8] in recent years. Synthetic magnetic flux or spin-orbit coupling are achieved by experimental techniques of laser-induced tunneling [3–7, 9] and lattice modulation techniques [8, 10, 11]. With regard to interacting systems, fermionic superfluid (superconducting) phases with salient orbital symmetry (such as p or d wave) [12, 13] have been actively searched for decades. They support edge-state fermions featuring non-Abelian braiding statistics [14] within the energy gap opened up along the Fermi surface.

Recently, the search for similar phenomena in bosonic systems, which are easier to implement with cold atomic gases, attracts broad interest. Several theoretical ideas [15–17] have been put forward to realize topological bosonic elementary excitations. One can utilize bosons condensed in the minimum of the lowest single-particle Bloch band, which is endowed with topological character by means of a synthetic gauge field [15, 16]. An alternative approach is based on the formation of a background vortex-lattice condensate with optical phase imprinting [17]. Both types of proposals imply significant experimental complexity.

In this Letter, we find that because of the interplay of interaction and orbital symmetry, topological elementary excitations naturally occur in a staggered chiral bosonic $p_x \pm ip_y$ superfluid discovered in a series of recent experiments at Hamburg [18–20]. We show that it supports Dirac bosons with π Berry flux in a higher lying branch of excitation spectrum. Surprisingly, we find that via adjusting the population imbalance of the $p_x + ip_y$ and $p_x - ip_y$ components, a topological phase transition occurs, accompanied by a bulk gap opening up near the Dirac cones. This leads to finite energy in-gap edge excitations for the finite system. Most strikingly, the topologically protected edge excitations are generated by the background chiral superfluid, which distinguishes this work from others that rely on engineering of the single-particle band structure. Below, we will discuss in detail how the required population imbalance tuning can be readily achieved with standard experimental techniques.

We thus realize a bosonic counterpart of topological chiral fermionic superfluidity, which is reminiscent of the famous example of topological superconductivity: the fermionic $p_x + ip_y$ state, believed to occur in strontium ruthenates [21, 22]. Their shared features include (1) both bosonic and fermionic superfluid states have nonzero global orbital angular momentum, and (2) both support topologically protected in-gap edge excitations. However, a fundamental difference exists. The fermionic state has a bulk gap above the ground state and supports zero modes at material edges or in vortex cores, while the bosonic superfluid has gapless Nambu-Goldstone modes immediately above the ground state due to the continuous global U(1) gauge symmetry breaking and the topological edge states occur inside a bulk gap at high energies.

Model. We employ a generalized version of the lattice geometry employed in earlier experiments [18–20] given by the potential $V(x,y) = V_H(x,y) + V_S(x,y)$ with

$$V_H(x,y) \;=\; -V_1 \left|\cos(k_L x) + e^{i\beta}\cos(k_L y)\right|^2 , \qquad (1)$$

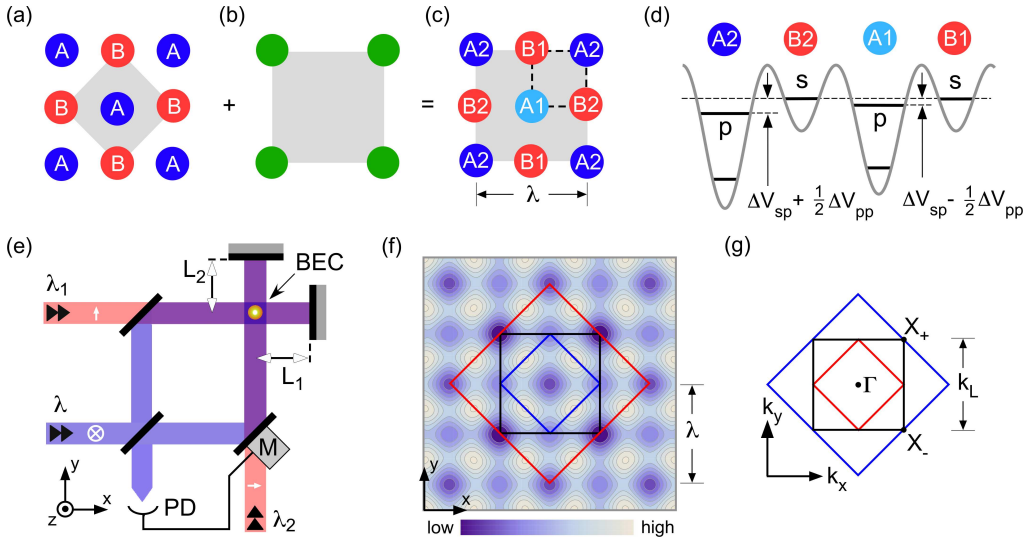

FIG. 1: (color online). (a) The checkerboard potential V_H comprises two classes of wells denoted A and B. (b) Geometry of the added square lattice V_S for the simplest case $\eta = 0$. (c) The complete lattice $V = V_H + V_S$ comprises four classes of sites denoted as $A1$, $A2$, $B1$, and $B2$. The gray rectangles in (a), (b), (c) indicates the unit cells of V_H, V_S, and V, respectively. (d), The potential V is shown along the dashed square in (c). The s and p orbitals accounted for in the tight binding model are indicated. (e) Laser beams at wavelengths λ, λ_1 and λ_2 are coupled to the interferometric setup for the formation of V. Their linear polarizations (orthogonal or parallel with respect to the xy plane) are indicated by white arrows. The phase β in Eq. (2) is servo-controlled by a movable mirror (M) and a photo detector (PD), in order to tune $\Delta V_{\rm sp}$ in Eq. (3). (f), Contour plot of the lattice potential $V = V_H + V_S$. The inner blue and middle black solid squares denote the unit cells of the lattice potential V_H and V, respectively. The outer red solid square denotes the unit cell of the predicted order parameter. (g), The first Brillouin zones corresponding to the unit cells shown in (f).

$$V_S(x,y) \;=\; V_2\left[\cos^2(\frac{1+2\eta}{2}k_L x)+\cos^2(\frac{1+2\eta}{2}k_L y)\right].$$

Here, V_H is the original lattice of the Hamburg experiments, which provides deep and shallow wells, denoted by A and B (see Fig. 1(a)). This lattice is formed by two interfering optical standing waves aligned along the x- and y-axes, respectively, with linear polarizations parallel to the z-axis, wavelength λ (with $k_L = 2\pi/\lambda$) and relative phase β, as detailed in Refs. [18–20, 23]. We superimpose an additional weak ($|V_2| \ll |V_1|$) conventional square lattice potential V_S as used in many experiments, with wave number $\frac{1+2\eta}{2}k_L$ and $\eta \in \{0, 1, 2, ...\}$ (see Fig. 1(b) for the case $\eta = 0$). V_S acts to subdivide the deep A-sites into two classes $(A1, A2)$ of slightly different depth.

In the tight-binding regime, by taking into account p_x and p_y orbitals in the deep $(A1, A2)$ and s orbitals in the shallow wells $(B1, B2)$, we model our system by the extended Hubbard Hamiltonian $\hat{H} = \hat{H}_0 + \hat{H}_{\rm int}$, where

$$\begin{aligned}\hat{H}_0 \;=\; & -J_{\rm sp}\sum_{\mathbf{r},\mu}\left[\hat{b}^\dagger_{\mu,\mathbf{r}}\hat{b}_{s,\mathbf{r}+\mathbf{e}_\mu}-\hat{b}^\dagger_{\mu,\mathbf{r}}\hat{b}_{s,\mathbf{r}-\mathbf{e}_\mu}+\text{h.c.}\right]\\ & +J_\parallel\sum_{\mathbf{r},\mu}\left[\hat{b}^\dagger_{\mu,\mathbf{r}}\hat{b}_{\mu,\mathbf{r}+\mathbf{e}_x+\mathbf{e}_y}+\hat{b}^\dagger_{\mu,\mathbf{r}}\hat{b}_{\mu,\mathbf{r}+\mathbf{e}_x-\mathbf{e}_y}+\text{h.c.}\right]\\ & +J_\perp\sum_{\mathbf{r},\mu}\left[\hat{b}^\dagger_{\mu,\mathbf{r}}\hat{b}_{\bar{\mu},\mathbf{r}+\mathbf{e}_x+\mathbf{e}_y}-\hat{b}^\dagger_{\mu,\mathbf{r}}\hat{b}_{\bar{\mu},\mathbf{r}+\mathbf{e}_x-\mathbf{e}_y}+\text{h.c.}\right]\\ & +\sum_{\mathbf{r}}\left[-\Delta V_{\rm sp}+\frac{1}{2}\Delta V_{\rm pp}(-)^{r_x+r_y}\right]\hat{n}_{p,\mathbf{r}}, \qquad (2)\end{aligned}$$

$$\begin{aligned}\hat{H}_{\rm int} \;=\; & \frac{U_s}{2}\sum_{\mathbf{r}}\hat{n}_{s,\mathbf{r}+\mathbf{e}_x}(\hat{n}_{s,\mathbf{r}+\mathbf{e}_x}-1)\\ & +\frac{U_p}{2}\sum_{\mathbf{r}}\left\{\hat{n}_{p,\mathbf{r}}\left[\hat{n}_{p,\mathbf{r}}-\frac{2}{3}\right]-\frac{1}{3}\hat{L}^2_{z,\mathbf{r}}\right\}. \qquad (3)\end{aligned}$$

Here, $\hat{b}_{s,\mathbf{r}'}$ and $\hat{b}_{\mu,\mathbf{r}'}$are bosonic annihilation operators for s and p_μ $(\mu = \{x, y\})$ orbitals at site $\mathbf{r}'$. The vector $\mathbf{r} = (r_x, r_y)\lambda$ with integer r_x and r_y denotes the position of p orbitals, while s orbitals are located at $\mathbf{r} + \mathbf{e}_\mu$ with $\mathbf{e}_x = (\lambda/2, 0)$ and $\mathbf{e}_y = (0, \lambda/2)$. $\bar{\mu} = \{\bar{x}, \bar{y}\} = \{y, x\}$. The number and the on-site angular momentum operators are respectively given by $\hat{n}_s = \hat{b}^\dagger_s\hat{b}_s$, $\hat{n}_p = \hat{b}^\dagger_x\hat{b}_x + \hat{b}^\dagger_y\hat{b}_y$, and $\hat{L}_z = -i(\hat{b}^\dagger_x\hat{b}_y - \hat{b}^\dagger_y\hat{b}_x)$. The $\Delta V_{\rm pp}$ term arises from the added potential V_S, which induces a staggered on-site energy shift for p orbitals at A sites.

For the single-particle Hamiltonian H_0, the band minima are located at $X_\pm = (1, \pm 1)k_L/2$ independent of V_S. This yields a finite-momentum condensate for weakly interacting bosons. The corresponding unit cell of the order parameter is enlarged by a factor of $\sqrt{2}$ and rotated by 45° with respect to that of the lattice potential $V = V_H + V_S$, hence is composed of four A and four B sites, as illustrated by the red solid square in Fig. 1(f). Ferro-orbital interaction favors a

special phase correlation between the two band minima, leading to a staggered on-site orbital angular momentum distribution with the relative phase between p_x and p_y orbitals fixed at $\pm\pi/2$ [24, 25]. Figure 2(a) shows the schematic representation of the ground-state order parameter. While previous studies concentrated on the chiral nature of such a p orbital bosonic superfluid, the present study investigates the elementary excitations on top of it instead. Remarkably, we find that interactions among bosons not only generate a ground state with chiral orbital order as is understood and experimentally confirmed, but also give rise to topological quasiparticle excitations to be described in the following.

Topological elementary excitations. We follow the standard number-conserving approach to obtain the excitation spectra [26]. Firstly, we focus on the symmetry of the Bogoliubov-de Gennes (BdG) Hamiltonian $\mathcal{H}(\mathbf{k})$. The presence of the staggered chiral orbital order breaks both time reversal and original lattice translation symmetries. Nevertheless, for $V_S = 0$, via choosing a specific global phase of the order parameter $\mathcal{H}(\mathbf{k})$ is invariant under the combined symmetry operations of time reversal $\mathcal{T}$ and lattice translations $\Theta_\pm$ along the $x \pm y$ directions by $\lambda/\sqrt{2}$: $\Theta_\pm\mathcal{T}\mathcal{H}(\mathbf{k})(\Theta_\pm\mathcal{T})^{-1} = \mathcal{H}(-\mathbf{k})$. The combined symmetries are described by anti-unitary operators $\Theta_\pm\mathcal{T}$ and are broken for $V_S \neq 0$. As will become clear later, this property plays an important role in the topological classification. The Hamiltonian is then diagonalized by a paraunitary matrix $T_\mathbf{k}$ as $T_\mathbf{k}^\dagger\mathcal{H}(\mathbf{k})T_\mathbf{k} = E_\mathbf{k}$, with eigenvalues contained in the diagonal terms of the diagonal matrix $E_\mathbf{k}$. To characterize the topological feature of the bosonic excitations, we follow the prescriptions of Refs. [27, 28] to define a topological invariant for the j-th excitation band in the reduced first Brillouin Zone (RFBZ) denoted by the red solid line in Fig. 1(g) as

$$\mathcal{C}_j = \frac{1}{2\pi}\int_{\mathrm{RFBZ}} d^2\mathbf{k} B_j(\mathbf{k}), \tag{4}$$

where the Berry curvature B_j and Berry connection $A_{j,\mu}$ are defined as $B_j(\mathbf{k}) \equiv \partial_{k_x}A_{j,y}(\mathbf{k}) - \partial_{k_y}A_{j,x}(\mathbf{k})$ and $A_{j,\mu}(\mathbf{k}) \equiv i\mathrm{Tr}[\Gamma_j T_\mathbf{k}^{-1}\tau_z(\partial_{k_\mu}T_\mathbf{k})]$. Γ_j is a diagonal matrix with the j-th diagonal term equals to 1 and other terms are 0, and $[\tau_z]_{ij}$ equals to δ_{ij} if $i = 1, ..., 12$ and $-\delta_{ij}$ otherwise [26].

We first consider the case of $V_S = 0$ corresponding to the recently reported experiments [18–20]. In this case, $A1$ and $A2$ sublattice sites are equivalent, and therefore are equally populated in the p orbital bands for the ground state. Fig. 2(b) summarizes numerical results for the parameters at $J_{\mathrm{sp}} = 0.12\,E_{\mathrm{rec}}$, $J_\parallel = 0.07\,J_{\mathrm{sp}}$, $J_\perp = 0.15\,J_{\mathrm{sp}}$, $\Delta V_{\mathrm{sp}} = 0.3\,J_{\mathrm{sp}}$, $U_s = 0.24\,E_{\mathrm{rec}}$, and $U_p = 0.12\,E_{\mathrm{rec}}$, all in units of $E_{\mathrm{rec}} = \hbar^2k_L^2/(2m)$. Only the lowest 8 energy bands along the high-symmetry lines are shown. These fully connected bands are gapped from the other 4 topologically trivial

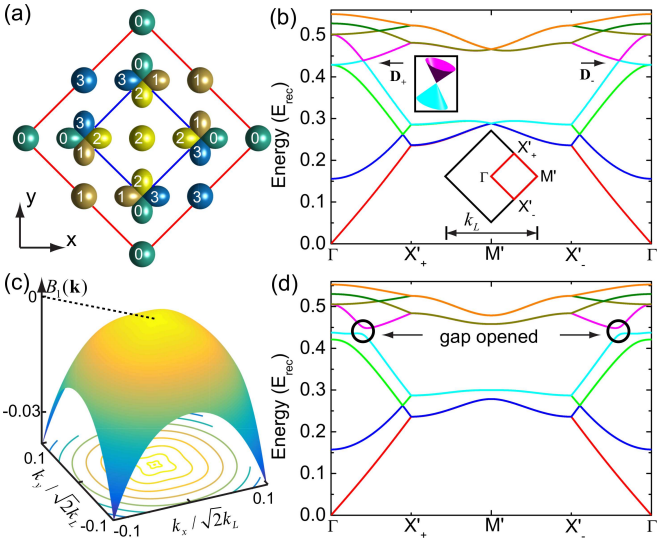

FIG. 2: (color online). (a) The schematic picture of the order parameter in one unit cell denoted by the outer solid square. The integer number ν denotes the phase of the orbital wavefunction as $\nu\,\pi/2$. Specifically, p orbitals are located at the four corners of the inner square, while other sites are occupied by the s orbitals. (b) Excitation spectra for $V_S = 0$ along the high-symmetric lines in the first Brillouin zone marked by the red diamond in the lower inset. Two Dirac points are denoted by D_+ and D_-. The parameters used in numerics are $J_{\mathrm{sp}} = 0.12\,E_{\mathrm{rec}}$, $J_\parallel = 0.07\,J_{\mathrm{sp}}$, $J_\perp = 0.15\,J_{\mathrm{sp}}$, $\Delta V_{\mathrm{sp}} = 0.3\,J_{\mathrm{sp}}$, $U_s = 0.24\,E_{\mathrm{rec}}$, $U_p = 0.12\,E_{\mathrm{rec}}$, and $\Delta_{\mathrm{pp}} = 0$. The mean boson density corresponds to one particle per orbital. Here, only the lowest 8 bands are shown. (c) Berry curvature of the first band of elementary excitation. (d) The same as (b) except a bias square optical lattice potential V_S is turned on to induce a population imbalance between $p_x + ip_y$ and $p_x - ip_y$ components, which opens a gap around the Dirac points leading to topological elementary excitations and nonzero Berry curvature for the phonon mode shown in (c). Here, the only difference in parameters used in numerics is $\Delta_{\mathrm{pp}} = 3\,\Delta_{\mathrm{sp}}$.

higher energy bands due to the relatively larger contact interaction energy for the s orbitals as compared to the p orbitals. Meanwhile, similar to a conventional Bose-Einstein condensate, the spontaneous breaking of U(1) phase symmetry guarantees the emergence of a phonon mode with linear dispersion close to $\mathbf{k} = \mathbf{0}$. We find the Berry curvature for this phonon mode to be negligible.

Surprisingly, an interesting feature in the excitations appears. Focusing on the 8 bands shown in Fig. 2(b), the 4-th and the 5-th bands are connected only at the four Dirac points located on the straight lines $\Gamma X'_\pm$ in momentum space. Two of them are denoted as $D_\pm$ and the other two correspond to their time-reversal points. Each of the Dirac points is associated with a π Berry flux such that in its vicinity the excitation spectrum depends linearly on momentum. This feature, which is analogous to fermionic topological semimetals studied in Refs. [29, 30], may be measured by applying Aharonov-

Bohm interferometry [31, 32].

Next, we consider the general case with $V_S \neq 0$. The order parameter shows the same phase correlation among s and p orbitals as for $V_S = 0$, which is illustrated in Fig. 2(a). The nonzero bias potential V_S causes the $A1$ and $A2$ lattice sites to be inequivalent and hence induces a population imbalance between them. No matter how small V_S is, a topological phase transition occurs. This is because the combined time reversal and discrete lattice translation symmetry $\Theta_{\pm}\mathcal{T}$ is broken for both the Hamiltonian and the order parameter, leading to a topological bulk gap on all Dirac points, as shown in Fig. 2(d). For $V_S \neq 0$, the total 12 excitation bands are separated into three groups. The four *connected* middle bands (5th-8th) are isolated by gap from four lower bands shown in Fig. 2(d) and four highest bands which are not shown. The summation of their topological invariants are well defined. Using Eq. (4), we confirm that the middle four bands are topological with $|\sum_{j=5}^{8}\mathcal{C}_j| = 2$. To further elucidate their topological behavior, we investigate the chiral edge states of the system for a cylinder geometry with a periodic (or open) boundary condition in the $x+y$ (or $x-y$) direction. For this finite system, the numerically obtained excitation spectra are plotted in Fig. 3. It clearly shows that topological edge states appear within the energy gap, connecting the upper and lower bulk states. The existence of two chiral edge states on each edge is consistent with the topological invariant being equal to 2 [1].

Refocusing on the phonon mode, we notice a striking feature appearing when $V_S \neq 0$. Different from the case of $V_S = 0$, the bias potential V_S induces a population imbalance for p orbitals on $A1$ and $A2$ sites, leading to a nonzero total orbital angular momentum together with a nonzero Berry curvature for the phonon mode. Specifically, as shown in Fig. 2(c), $B_1(\mathbf{k})$ is zero at the Γ point and negative everywhere else in the $\mathbf{k}$-space area displayed, a situation implicating the existence of a phonon Hall effect [33].

Based on the above results, we understand that the population imbalance between the clockwise and the counter-clockwise orbiting condensate components is key to the appearance of topological elementary excitations in the p band bosonic superfluid. The underlining symmetry for characterizing this imbalance is $\Theta_{\pm}\mathcal{T}$. To verify that this is indeed generally true rather than being specific to the form of V_S used, we apply two other methods capable of opening a bulk gap close to the Dirac points [26]. The first one is to introduce an asymmetry between the s-p orbital hopping amplitudes along two orthogonal directions, e.g., along the x- and y-axis, which corresponds to adding the following term $\hat{H}_1 = -\Delta J_{\rm sp}\sum_{\mathbf{r}}\left[\hat{b}_s^{\dagger}(\mathbf{r})\hat{b}_y(\mathbf{r}+\mathbf{e}_y) + \hat{b}_s^{\dagger}(\mathbf{r})\hat{b}_y(\mathbf{r}-\mathbf{e}_y) + \text{h.c.}\right]$ to the system Hamiltonian. The second one is to generate an on-site rotation described by the Hamiltonian $\hat{H}_2 = i\Omega_z\sum_{\mathbf{r}}\left[\hat{b}_x^{\dagger}(\mathbf{r})\hat{b}_y(\mathbf{r}) - \hat{b}_y^{\dagger}(\mathbf{r})\hat{b}_x(\mathbf{r})\right]$. Our numerical calculations indeed confirm that the first method creates a trivial gap because it does not break the $\Theta_{\pm}\mathcal{T}$ symmetry, while the second method relying on the on-site rotation breaks $\mathcal{T}$, thus breaks $\Theta_{\pm}\mathcal{T}$, giving rise to similar topological excitation bands as shown in Figs. 2(d) and 3.

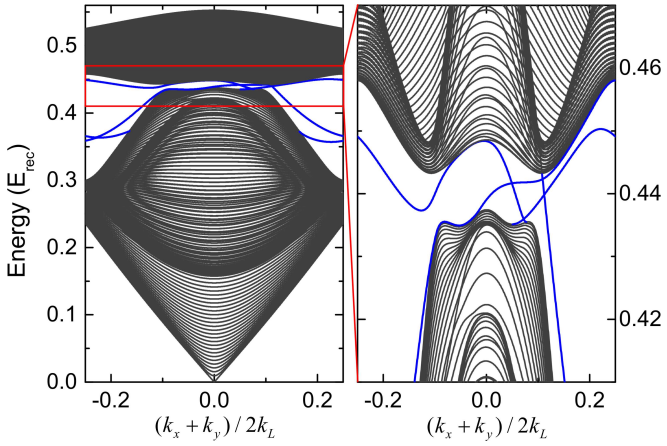

FIG. 3: (color online). Elementary excitation spectra for a finite system with a cylinder geometry. A periodic (open) boundary condition is assumed in the $x+y$ ($x-y$) direction. One unit cell of the finite system contains 40 copies of the unit cell of the order parameter. The lattice potential and interaction parameters are the same as that used in Fig. 2(d). Solid black and blue lines denote the bulk excitation spectra and the chiral edge states, respectively.

Experimental realization and detection. A schematic experimental setup for investigating our proposed study is shown in Fig. 1(e). The weak V_S can be realized by including two additional laser beams with linear polarizations within the xy plane and wavelengths $\lambda_n = \lambda' + \delta\lambda_n$ with $\lambda' \equiv \frac{2}{1+2\eta}\lambda$. Take $\lambda = 1064\,\text{nm}$ and $\eta = 1$, $\lambda' \approx 709\,\text{nm}$, a wave length for which laser light is readily available. The small quantities $\delta\lambda_n, n \in \{1,2\}$ are chosen according to the distances L_n in Fig. 1(e), in order to precisely adjust the relative positions of both lattices. Assuming $L_1 = L_2 = 20\,\text{cm}$ a shift of V_S by half a lattice constant amounts to $c/\delta\lambda_n = 375\,\text{MHz}$ with c denoting the speed of light. Technically, it is easily possible to fix $c/\delta\lambda_n$ with a precision of a few MHz such that the relative positions of the lattices can be adjusted to better than a few nm [26]. As discussed in Ref. [34], the bias potential may also induce a staggered on-site coupling between p_x and p_y orbitals. However, such a coupling is proportional to the second derivative of the bias lattice potential, which is negligible for the weak lattice potential required here, e.g., $\Delta V_{\rm pp} \sim J_{\rm sp}$. The topological features of the elementary excitations can be experimentally measured via coherently transferring a small portion of the condensate into an edge mode by stimulated Raman transitions [26, 35]. As the

relation between the original bosons and the elementary excitations are connected by the paraunitary matrix $T_{\mathbf{k}}$, the interference of the edge mode and the condensate wavefunction is predicted to form a density wave for the original bosons along the edge [26], by the same mechanism discussed in Ref. [16].

Conclusion. We study the elementary excitations of the staggered chiral $p_x \pm ip_y$ orbital superfluid realized in the Hamburg experiments [18–20]. We find that for the experimentally implemented lattice configuration, the elementary excitations are not topologically gapped due to the presence of the combined symmetries $(\Theta_{\pm}\mathcal{T})$, whose topological classification falls into the BDI class [1] after taking into account the intrinsic particle-hole symmetry of $\tau_z\mathcal{H}(\mathbf{k})$. Four Dirac cones are found in the higher lying excitation spectrum. In constrast, when a bias square lattice potential imbalances the $p_x + ip_y$ and $p_x - ip_y$ components, a striking, unexpected topological phase transition appears. The resulting superfluid state supports topological gapped bulk elementary excitations accompanied by in-gap topologically protected edge excitations. This finding extends current research on topological phases of fermionic atoms and electrons to weakly interacting Bose atoms. Most significantly, the chiral orbital order and the topological elementary excitations we discuss are driven by the many-body interaction, which is in contrast to those requiring single-particle Bloch bands with topological character.

This work is supported by NSFC (No. 11574100) (ZFX), 2013CB922004 of the National Key Basic Research Program of China, and by NSFC (No. 91121005, No. 91421305) (LY), and U.S. ARO (W911NF-11-1-0230), AFOSR (FA9550-16-1-0006), the Charles E. Kaufman Foundation and The Pittsburgh Foundation, Overseas Collaboration Program of NSF of China (No. 11429402) sponsored by Peking University, and National Basic Research Program of China (No. 2012CB922101) (WVL). AH acknowledges support by DFG-SFB925 and the Hamburg centre of ultrafast imaging (CUI). ZFX is also supported in part by the National Thousand-Young-Talents Program.

* Electronic address: zfxu83@gmail.com
† Electronic address: wvliu@pitt.edu

[1] M. Z. Hasan and C. L. Kane, Rev. Mod. Phys. **82**, 3045 (2010).
[2] X. L. Qi and S.-C. Zhang, Rev. Mod. Phys. **83**, 1057 (2011).
[3] M. Aidelsburger, M. Atala, M. Lohse, J. T. Barreiro, B. Paredes, and I. Bloch, Phys. Rev. Lett. **111**, 185301 (2013).
[4] H. Miyake, G. A. Siviloglou, C. J. Kennedy, W. C. Burton and W. Ketterle, Phys. Rev. Lett. **111**, 185302 (2013).
[5] M. Aidelsburger, M. Lohse, C. Schweizer, M. Atala, J. T. Barreiro, S. Nascimbène, N. R. Cooper, I. Bloch, and N. Goldman, Nature Physics **11**, 162-166 (2015).
[6] M. Mancini, G. Pagano, G. Cappellini, L. Livi, M. Rider, J. Catani, C. Sias, P. Zoller, M. Inguscio, M. Dalmonte, and L. Fallani, Science **349**, 1510 (2015).
[7] B. K. Stuhl, H.-I. Lu, L. M. Aycock, D. Genkina, and I. B. Spielman, Science **349**, 1514 (2015).
[8] G. Jotzu, M. Messer, R. Desbuquois, M. Lebrat, T. Uehlinger, D. Greif, and T. Esslinger, Nature **515**, 237 (2014).
[9] Y.-J. Lin, K. Jiménez-Garcia, and I. B. Spielman, Nature **471**, 83 (2011).
[10] J. Struck, C. Ölschläger, R. Le Targat, P. Soltan-Panahi, A. Eckardt, M. Lewenstein, P. Windpassinger, and K. Sengstock, Science **333**, 996 (2011).
[11] C. V. Parker, L. C. Ha, and C. Chin, Nature Physics **9**, 769 (2013).
[12] G. E. Volovik, The universe in a helium droplet, Oxford University Press, (2003).
[13] C. Kallin, Rep. Prog. Phys. **75**, 042501 (2010).
[14] C. Nayak, S. H. Simon, A. Stern, M. Freedman, and S. Das Sarma, Rev. Mod. Phys. **80**, 1083 (2008).
[15] G. Engelhardt and T. Brandes, Phys. Rev. A **91**, 053621 (2015).
[16] S. Furukawa and M. Ueda, New J. Phys. **17**, 115014 (2015).
[17] C.-E. Bardyn, T. Karzig, G. Refael, and T. C. H. Liew, Phys. Rev. B **93**, 020502(R) (2016).
[18] G. Wirth, M. Ölschläger, and A. Hemmerich, Nature Physics **7**, 147 (2011).
[19] M. Ölschläger, T. Kock, G. Wirth, A. Ewerbeck, C. M. Smith, and A. Hemmerich, New J. Phys. **15**, 083041 (2013).
[20] T. Kock, M. Ölschläger, A. Ewerbeck, W.-M. Huang, L. Mathey, and A. Hemmerich, Phys. Rev. Lett. **114**, 115301 (2015).
[21] Y. Maeno, H. Hashimoto, K. Yoshida, S. Nishizaki, T. Fujita, J. G. Bednorz, and F. Lichtenberg, Nature **372**, 532 (1994).
[22] A. P. Mackenzie and Y. Maeno, Rev. Mod. Phys. **75**, 657 (2003).
[23] A. Hemmerich, D. Schropp, and T. W. Hänsch, Phys. Rev. A **44**, 1910 (1991).
[24] A. Isacsson and S. M. Girvin, Phys. Rev. A **72**, 053604 (2005).
[25] W. V. Liu and C. Wu, Phys. Rev. A **74**, 013607 (2006).
[26] See Supplemental Material which includes Refs. [36–41] for additional details on single-particle energy spectra, methods for the derivation of elementary excitations, two alternative schemes to open a bulk gap, alightment of two optical lattices, and edge-state detection.
[27] J. E. Avron, R. Seiler, and B. Simon, Phys. Rev. Lett. **51**, 51 (1983).
[28] R. Shindou, R. Matsumoto, S. Murakami, and J.-i. Ohe, Phys. Rev. B **87**, 174427 (2013).
[29] A. H. Castro Neto, F. Fuinea, N. M. R. Peres, K. S. Novoselov, and A. K. Geim, Rev. Mod. Phys. **81**, 109 (2009).
[30] K. Sun, W. V. Liu, A. Hemmerich, S. Das Sarma, Nature Physics **8**, 67 (2012).
[31] M. Atala, M. Aidelsburger, J. T. Barreiro, D. Abanin, T. Kitagawa, E. Demler, and I. Bloch, Nature Physics **9**, 795 (2013).
[32] L. Duca, T. Li, M. Reitter, I. Bloch, M. Schleier-Smith,

and U. Schneider, Science **347**, 288 (2015).
[33] D. Xiao, M.-C. Chang, and Q. Niu, Rev. Mod. Phys. **82**, 1959-2007 (2010).
[34] X. Li, A. Paramekanti, A. Hemmerich, and W. V. Liu, Nature Communications **5**, 3205 (2014).
[35] P. T. Ernst, S. Götze, J. S. Krauser, K. Pyka, D.-S. Lühmann, D. Pfannkuche, and K. Sengstock, Nature Physics **6**, 56 (2010).
[36] L. Tarruell, D. Greif, T. Uehlinger, G. Jotzu, and T. Esslinger, Nature **483**, 302 (2012).
[37] N. Gemelke, E. Sarajlic, and S. Chu, arXiv:1007.2677.
[38] M. Zhang, H.-h. Hung, C. Zhang, and C. Wu, Phys. Rev. A **83**, 023615 (2011).
[39] G.-B., Jo, J. Guzman, C. K. Thomas, P. Hosur, A. Vishwanath, and D. M. Stamper-Kurn, Phys. Rev. Lett. **108**, 045305 (2012).
[40] S. Taie, H. Ozawa, T. Ichinose, T. Nishio, S. Nakajima, and Y. Takahashi, Sci. Adv. **1**, e1500854 (2015).
[41] A. L. Gaunt, T. F. Schmidutz, I. Gotlibovych, R. P. Smith, and Z. Hadzibabic, Phys. Rev. Lett. **110**, 200406 (2013).